Journal of Magnetic Resonance 310 (2020) 106639

Contents lists available at ScienceDirect

Journal of Magnetic Resonance

journal homepage: www.elsevier.com/locate/jmr

De novo resonance assignment of the transmembrane domain of LR11/SorLA in *E. coli* membranes

Xiaoyan Ding [a], Riqiang Fu [b,*], Fang Tian [a,*]

[a] Department of Biochemistry and Molecular Biology, The Pennsylvania State University, Hershey, PA 17033, USA
[b] National High Magnetic Field Laboratory, 1800 East Paul Dirac Dr., Tallahassee, FL 32310, USA

ARTICLE INFO

Article history:
Received 13 August 2019
Revised 28 October 2019
Accepted 30 October 2019
Available online 1 November 2019

Keywords:
Membrane protein
Solid-state NMR
Inner membrane
Reverse labeling
Frequency-selective dipolar dephasing
Difference spectroscopy

ABSTRACT

Membrane proteins perform many important cellular functions. Historically, structural studies of these proteins have been conducted in detergent preparations and synthetic lipid bilayers. More recently, magic-angle-spinning (MAS) solid-state NMR has been employed to analyze membrane proteins in native membrane environments, but resonance assignments with this technique remain challenging due to limited spectral resolution and high resonance degeneracy. To tackle this issue, we combine reverse labeling of amino acids, frequency-selective dipolar dephasing, and NMR difference spectroscopy. These methods have resulted in nearly complete resonance assignments of the transmembrane domain of human LR11 (SorLA) protein in *E. coli* membranes. To reduce background signals from *E. coli* lipids and proteins and improve spectral sensitivity, we effectively utilize amylose affinity chromatography to prepare membrane vesicles when MBP is included as a fusion partner in the expression construct.

1. Introduction

Sophisticated methods for using magic-angle-spinning (MAS) solid-state NMR (ssNMR) to characterize membrane proteins in biological membrane environments have been developed in the past decade [1–5]. Both isolated membrane vesicles (*in situ*) and intact cells (*in-cell*) can be used effectively with MAS ssNMR. With targeted sample preparation aimed at reducing the signals of background lipids and proteins [6,7] and ^{1}H-detection and dynamic nuclear polarization (DNP) techniques to improve spectral sensitivity [8–17], *in situ* and *in-cell* ssNMR have provided unique insights into the effects of complex biological membranes on the structure and dynamics of membrane proteins and their complexes [18–24]. For example, ssNMR studies of M2 [25], DAGK [26], PagL [27], Mistic [16], CsmA [28], ASR (*Anabaena* sensory rhodopsin) [7], and Aquaporin Z [29] in biological membranes validated structures that were previously determined using model membrane systems. In contrast, spectral differences of Yidc in *E. coli* membrane vesicles and in reconstituted proteoliposomes indicated that protein conformation and dynamics likely differ in *E. coli* cells [30]. In most of these studies, resonance assignments of *in situ* ssNMR spectra were transferred from their assignments in model membrane systems, and *de novo* assignments proved difficult due to limited spectral resolution.

The inherent challenges of assigning *in situ* ssNMR spectra are illustrated by our study of the transmembrane domain (TM) of human LR11 (SorLA) in *E. coli* membrane vesicles. LR11 is a neuronal type I transmembrane protein that regulates the trafficking and processing of human amyloid precursor protein, which is central to the pathology of Alzheimer's disease [31–34]. Despite the fact that we were able to assign ~50% of LR11 TM residues with ^{13}C-^{13}C homonuclear correlation experiments in our early study [35], assigning remaining residues has been arduous. The ^{13}C resonance linewidth is ~1 ppm in our *in situ* NMR spectra, but the ^{15}N linewidth is >2.0 ppm despite our extensive efforts to optimize sample preparation and experimental conditions for NMR data collection. The measured ^{15}N transverse relaxation time of approximately 6 ms on a 600 MHz instrument (14.1 T) indicates that ^{15}N resonances suffer from heterogeneous broadening, most likely due to the complex *E. coli* membrane environment. As a result, standard 3D assignment experiments such as CANCO, CONCA, NCACX, and NCOCX are not effective. Additionally, the LR11 TM domain is rich in hydrophobic amino acids including Leu and Val, which cause severe spectral overlap. Amino acid selective labeling [36], a technique commonly used to reduce the number of observed resonances, is not effective in situations like these since ^{13}C chemical shifts of a particular amino acid usually overlap in the same spectral region. Amino acid ^{13}C-^{15}N pairwise labeling is

* Corresponding authors.
E-mail addresses: rfu@magnet.fsu.edu (R. Fu), ftian@psu.edu (F. Tian).

https://doi.org/10.1016/j.jmr.2019.106639
1090-7807/

useful but expensive. Here, we report on tackling these difficulties by using a combination of the reverse amino acid labeling strategy [37–40], spectral editing techniques [41–48], and difference spectroscopy. And, by taking advantage of the maltose-binding protein (MBP) fusion protein, we have been able to conveniently and effectively use amylose affinity chromatography to prepare inner membrane (IM) vesicles that contain our targeted protein. This approach to sample preparation has improved spectral sensitivity and the suppression of background signals from *E. coli* lipids and proteins.

2. Materials and methods

LR11 TM was expressed in *E. coli* BL21 CodonPlus (DE3) RIPL cells using a MBP expression vector according to procedures described previously [35,49]. Briefly, cells were grown in 4–5 mL LB medium at 37 °C overnight and then inoculated in 250 mL M9 medium supplied with ^{13}C- D-glucose (4 g/L) (Cambridge Isotope Laboratories) and ^{15}N-NH_4Cl (1 g/L) (Sigma-Aldrich). For amino acid reverse labeling samples, natural abundance amino acids (1 g/L) were added to ^{13}C/^{15}N M9 media. Protein expression was induced at OD_{600nm} of 0.6–0.9 with 1 mM Isopropyl β-D-1-thiogalactopyranoside (IPTG) at 16 °C for ~24 h. Cells were harvested by centrifugation and stored at −80 °C until use.

For the preparation of LR11 TM in *E. coli* membrane vesicles, cells were incubated on ice for 20 min and then resuspended in a lysis buffer containing 20 mM Tris-HCl, 500 mM NaCl, pH 8.0, ready-Lyse™ Lysozyme (30 mg/L), and OmniCleave™ Endonuclease (Epicentre, 250 units/L). The cell suspension was sonicated on ice for a total 6 min with 3 s on and 7 s off. The cell lysate was centrifuged at ~30,000*g* for 20 min to remove insolubles. For the preparation of crude membrane samples, the supernatant was mixed directly with 300–500 units thrombin (EMD Millipore Corp) and slowly rotated overnight at room temperature to cleave the MBP fusion protein completely. For the preparation of IM samples, the supernatant was loaded onto a column containing 3–5 mL amylose resin. After incubation for 1–2 h, the column was washed with 80 mL PBS buffer containing 10 mM Na_2HPO_4, 1.8 mM KH_2-PO4, pH 7.3, 137 mM NaCl, and 2.7 mM KCl. LR11 TM in IM vesicles was eluted with a PBS buffer containing 30 mM maltose. The elute was then mixed with 300–500 units of thrombin and slowly rotated overnight at room temperature to cleave the MBP fusion protein. Membrane pellets were isolated by ultracentrifugation at ~160,000*g* for 1 h, and washed several times with a buffer of 20 mM Hepes, pH 7.0, and 50 mM NaCl to further remove residual cleaved MBP. About 30 mg sample was packed into a 3.2 mm rotor for ssNMR experiments.

All NMR experiments were carried out on Bruker 500 MHz Avance II, 600 MHz Avance II or 800 MHz Avance III spectrometers using an E-free or home-made low-E 3.2 mm HCN triple-resonance MAS probe. Fig. 1 shows the pulse sequences used in our experiments. In the rotational-echo-double-resonance (REDOR)-edited $^{13}C_\alpha$-$^{13}C'$ correlation experiment (Fig. 1(a)), $^{13}C_\alpha$ resonances are selected after the cross-polarization (CP) from ^{1}H to ^{13}C and evolved in the t_1 dimension, followed by the magnetization transfer from $^{13}C_\alpha$ to ^{13}C' by radio frequency-driven recoupling (RFDR) [50]. A $^{13}C'$-^{15}N dipolar dephasing period, during which the $^{13}C'$-^{15}N dipolar interactions are reintroduced by the REDOR sequence [43], followed by a Z-filter, is inserted before detection. As a result, the resonance intensity of $^{13}C_\alpha$-$^{13}C'$ cross-peaks preceding ^{15}N-labeled residues is greatly reduced while the intensity of $^{13}C_\alpha$-$^{13}C'$ cross-peaks preceding unlabeled residues (which contain ^{14}N) remains unchanged. When the REDOR dephasing is off, spectra similar to conventional $^{13}C_\alpha$-$^{13}C'$ correlation spectra are produced. Fig. 1(b) is the pulse sequence for the frequency-selective dipolar recoupling (FDR)-edited NCA experiment [45]. In this sequence, after ^{1}H to ^{15}N cross-polarization, a $^{13}C'$-^{15}N FDR dephasing period [51] followed by a Z-filter, is introduced before the ^{15}N magnetization is evolved in the t_1 dimension and then transferred to $^{13}C_\alpha$ for detection. As a result, most of the intensity of the ^{15}N-$^{13}C_\alpha$ cross-peaks succeeding $^{13}C'$-labeled residues is reduced, while the intensity of the ^{15}N-$^{13}C_\alpha$ cross-peaks succeeding unlabeled residues (which contain ^{12}C) is minimally affected. Unless otherwise indicated, a ramped cross-polarization (CP) [52] of 500 μs with an 80–100% linear amplitude was used and the SPINAL decoupling sequence [53] with a ^{1}H radiofrequency field (RF) of 100 kHz was applied for proton decoupling. Typical 90° RF pulse lengths were set to 4 μs for the ^{13}C channel, 4.5 μs for the ^{15}N channel and 2.5 μs for the ^{1}H channel. The ^{13}C chemical shifts were referenced to the carbonyl carbon of glycine at 178.5 ppm (instead of 176.4 ppm used in our previous work) and the ^{15}N chemical shifts were referenced indirectly accordingly to the gyromagnetic ratio of ^{15}N/^{13}C. NMR data were processed and analyzed with Topspin software.

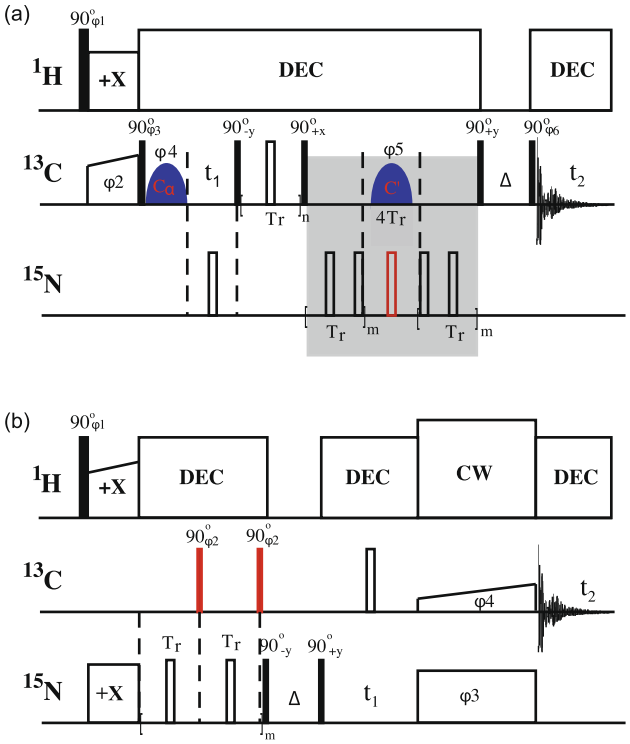

Fig. 1. Pulse sequences for spectral editing. (a) REDOR-edited $^{13}C_\alpha$-$^{13}C'$ correlation. The first Gaussian 90° pulse (blue) is used to select C_α resonances for evolution in the t_1 dimension, while the second Gaussian 180° (blue) is applied to the C' region. The 180° pulse in red on the ^{15}N channel is used to turn the $^{13}C'$-^{15}N dipolar recoupling on or off. Without this pulse, the $^{13}C'$-^{15}N dipolar couplings are refocused and no $^{13}C'$-^{15}N dipolar dephasing takes place. When this pulse is applied, the $^{13}C'$-^{15}N dipolar couplings are reintroduced, resulting in dephasing $^{13}C'$ resonances in $^{13}C'$-^{15}N spin pairs. A Z-filter is used before detection to ensure that only signals originating from the longitudinal magnetization are recorded in the t_2 dimension. The phase cycling is: ϕ1 = 1 3; ϕ2 = 0 0 2 2 2 2 0 0; ϕ3 = 1 1 3 3; ϕ4 = 3 3 1 1; ϕ5 = 1 3 1 3 3 1 3 1; ϕ6 = 0 0 0 0 0 0 0 0 2 2 2 2 2 2 2 2; and the receiver phase = 0 2 2 0 2 0 0 2 2 0 0 2 0 2 2 0. (b) FDR-edited ^{15}N-$^{13}C_\alpha$ correlation, where the red 90° pulses on the ^{13}C channel turn the $^{13}C'$-^{15}N dipolar dephasing on or off. Without these pulses, no $^{13}C'$-^{15}N dipolar dephasing takes place. With these pulses, the recoupled dipolar interactions attenuate ^{15}N resonances in $^{13}C'$-^{15}N spin pairs. The phase cycling is: ϕ1 = 1 3; ϕ2 = 0 2 0 2 0 2 0; ϕ3 = 0; ϕ4 = 0 0 2 2 1 1 3 3; and the receiver phase = 0 2 2 0 1 3 3 1. (For interpretation of the references to colour in this figure legend, the reader is referred to the web version of this article.)

3. Results and discussion

3.1. Reducing E. coli background signals and improving spectral sensitivity

The success of *in situ* ssNMR relies on careful sample preparation that minimizes NMR signals from background proteins and lipids so that most observed resonances are from targeted molecules. Early studies of bacteriorhodopsin (bR) benefited from the fact that bR is the most abundant component of the purple membrane (75%) [54]. Applying a similar logic, in 2011 we optimized conditions to maximize the expression of human LR11 TM in bacteria and characterized its secondary structure in *E. coli* membranes [35,49]. Subsequently, Baker et al. employed rifampicin to reduce endogenous protein expression during the induction of recombinant protein expression [6]; this created "isotopically" invisible *E. coli* background signals. However, when applied to our system, this approach significantly reduced the expression of LR11 TM. Other researchers have minimized background signals by using a sucrose gradient and a metal affinity two-phase separation method to selectively enrich membrane vesicles that contain targeted proteins [7,27,55,56]. The envelope of *E. coli* includes two distinct bilayers, the outer (OM) and inner membranes (IM), and the OM accounts for ~2/3 of the mass of crude membranes [57]. Our targeted proteins are expressed in IM. Separating IMs from OMs not only reduces *E. coli* background signals from lipopolysaccharides and outer membrane proteins but also allows more LR11 TM protein to be packed into a MAS rotor for better sensitivity. Since LR11 TM is expressed as an MBP fusion protein (Fig. 2a) [49,58], we used amylose affinity chromatography to prepare IM vesicles that contain our target (MBP-LR11 TM) before enzymatic cleavage of its fusion partner. Fig. 2(b) shows SDS-PAGE gel analyses of LR11 TM preparations in *E. coli* crude membranes (IM + OM) and IM vesicles. Compared to the crude membrane preparation (lane 2), IM vesicles eluted from an amylose affinity column clearly show an enrichment of targeted proteins relative to the *E. coli* backgrounds (lane 3). Fig. 2(c) and (d) show comparisons of 1D ^{13}C direct polarization and 2D ^{13}C-^{13}C correlation spectra of ^{13}C, ^{15}N-labeled LR11 TM in crude and IM preparations, respectively. An overlay of 1D ^{13}C CPMAS spectra is shown is Fig. S1. Signals around 70 and 100 ppm from *E. coli* OM lipopolysaccharides are greatly reduced in the IM preparation. Furthermore, a comparison of cross-peak intensities in Fig. 2(d) indicates ~60% improvement in spectral sensitivity.

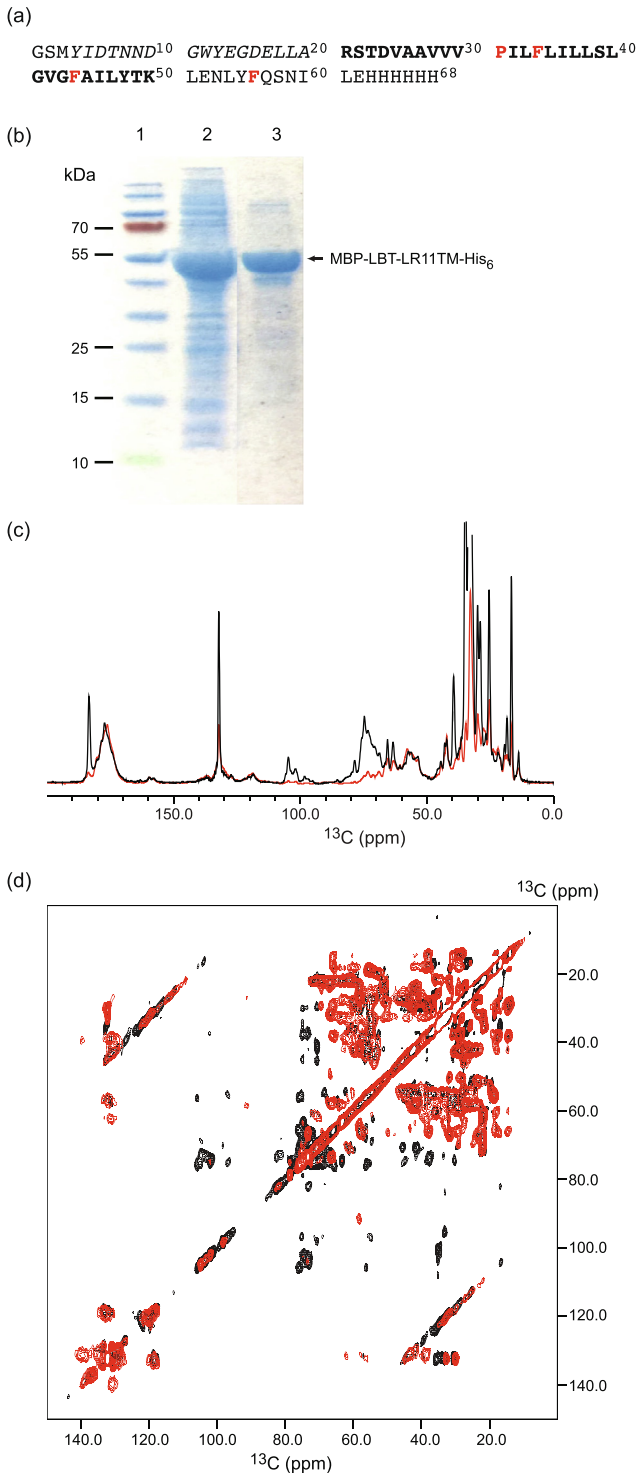

Fig. 2. (a) Primary sequence of the LBT-LR11TM-His$_6$. The LR11 fragment is shown in bold, corresponding to residues 2132–2161 of the full-length protein. The LBT (lanthanide binding tag) is shown in italics. Pro and Phe residues selected for unlabeled amino acid are colored red. (b) SDS-PAGE results of LR11 TM preparations in *E. coli* crude (lane 2) and inner (lane 3) membrane vesicles. Inner membrane vesicles were isolated using an amylose affinity column. (c) An overlay of 1D ^{13}C direct polarization MAS spectra of ^{13}C, ^{15}N-labeled LR11 TM in crude (black) and inner (red) membrane vesicles. (d) An overlay of 2D ^{13}C-^{13}C PARIS MAS spectra of ^{13}C, ^{15}N-labeled LR11 TM in crude (black) and inner (red) membrane vesicles. 2D spectra were recorded with a mixing time of 30 ms at a calibrated sample temperature of 293 K on a Bruker 500 MHz spectrometer. 128 t_1 and 512 t_2 complex points were acquired with a spectral width of 37.5 kHz for both dimensions, and the States method was used for quadrature detection in the F1 dimension. The MAS rate was 10 kHz. A two-pulse phase modulation (TPPM) scheme with a ^{1}H radiofrequency field of 100 kHz [60] was applied for proton decoupling during detection. The FIDs were apodized with a 60° shifted sine-bell function in both dimensions and zero-filled into a 256 × 2048 matrix before Fourier transformation. (For interpretation of the references to colour in this figure legend, the reader is referred to the web version of this article.)

3.2. Assigning LR11 TM resonances

Fig. 3(a, left) shows a $^{13}C_\alpha$-$^{13}C'$ correlation spectrum of LR11 TM in *E. coli* IM vesicles. The spectral resolution allows for the putative identification of a few amino acid types but is not sufficient for assigning individual LR11 TM residues that are abundant in Leu and Val. Multiple dimensional NMR is commonly used to improve spectral resolution. In this case, due to broad ^{15}N resonance linewidth (>2 ppm), spectral resolution and sensitivity of standard 3D assignment experiments suffer dramatically and provide little information for additional assignments beyond what were obtained previously. Recently, a combination of reverse amino acid labeling and spectral editing was used to overcome spectral

overlap for resonance assignments in proteoliposomes [45] and crystalline samples [46]. Fig. 3 shows $^{13}C_{\alpha}$-$^{13}C'$ correlation spectra of a ^{13}C, ^{15}N-labeled, Pro-unlabeled LR11 TM in *E. coli* IM vesicles using the pulse sequence shown in Fig. 1(a). When the REDOR dephasing is on, most resonance intensity is significantly reduced by the recoupled $^{13}C'$-^{15}N dipolar interactions, as shown in Fig. 3 (a, right). Contrary to our expectation of a single peak (because there is only one proline residue in our construct and proline does not interconvert to other amino acids, no isotope scrambling is expected [40]), multiple peaks are observed despite the fact that a cross-peak at 175.5, 70.0 ppm becomes more intense relative to other resonances. Three sample slices from Fig. 3(a) are shown in Fig. 3(b). While the peaks in slices from ^{13}C = 54.3 and 58.1 ppm show ~75% reductions in intensity as a result of the REDOR dephasing, a peak at 175.5 ppm in a slice from ^{13}C = 70.0 ppm displays similar resonance intensity. This suggests that this peak originates from Val30, the residue preceding Pro31. However, the residual intensity of the REDOR dephasing from overlapping resonances remains strong and it is difficult to identify a correct cross-peak for assignment (Fig. 3(a), right).

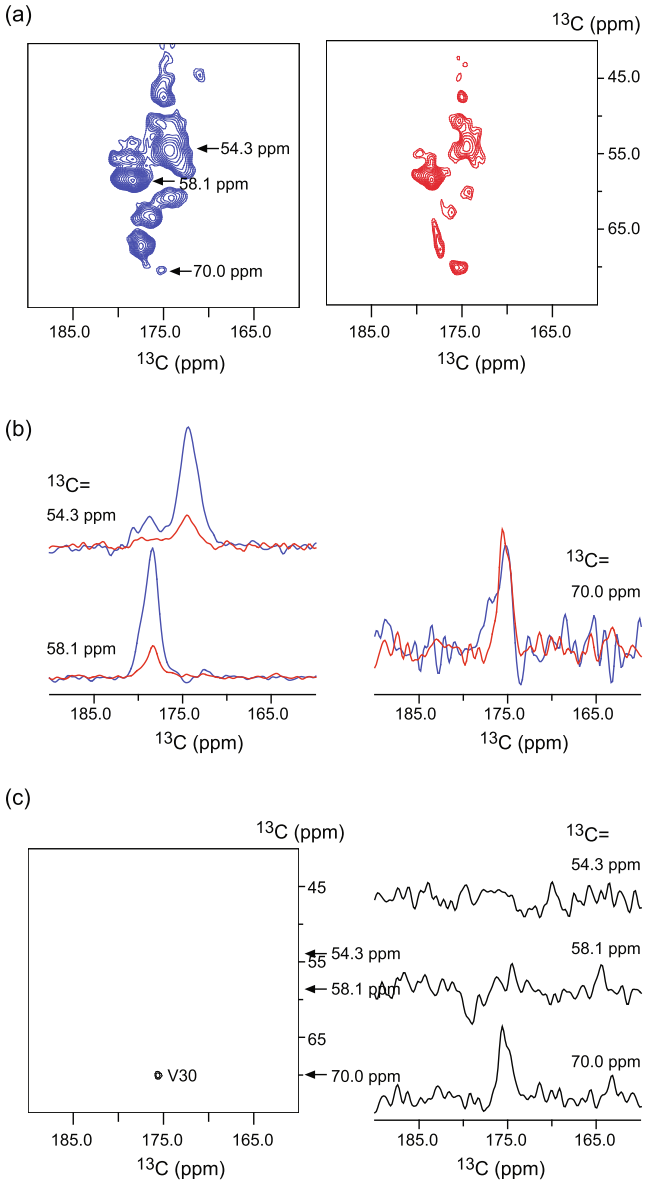

A shifted REDOR sequence has been developed to minimize the residual intensity from incomplete dephasing [59]. However, in practice it is difficult to choose one particular dephasing time that will suppress all background signals to zero, especially when small amounts of unlabeled amino acid scrambling are present. Here we use NMR difference spectroscopy to remove the residual intensity. The $^{13}C_{\alpha}$-$^{13}C'$ spectrum with the REDOR dephasing off (Fig. 3(a), left) was used as an approximation of the residual spectrum and subtracted from Fig. 3(a, right). This is a reasonable approach considering that differences in $^{13}C'$-^{15}N dipolar interactions of LR11 TM residues are likely small since they are embedded in lipid bilayers, and that small differences in their $^{13}C'$-^{15}N dipolar couplings have minor effects on the efficiency of the REDOR dephasing. The resulting difference spectrum is shown in Fig. 3(c) (the same spectrum at a low contour level is shown in Fig. S2). A single cross-peak at 175.5 and 70 ppm is observed and readily assigned to Val30.

To observe and assign residues succeeding unlabeled amino acids, Fig. 4 shows FDR-edited ^{15}N-$^{13}C_{\alpha}$ correlation spectra of a ^{13}C, ^{15}N-labeled, Pro-unlabeled LR11 TM in IM vesicles. When the FDR dephasing is off, it is similar to conventional ^{15}N-$^{13}C_{\alpha}$ correlation spectra (Fig. 4(a), left). When the FDR dephasing is on, resonance intensity is significantly reduced (Fig. 4(a), right). Again, contrary to our expectation of a single peak, multiple peaks are observed. Three sample slices from Fig. 4(a) are shown in Fig. 4 (b). All peaks in these slices show ~80% reductions in intensity as a result of the FDR dephasing except one peak at 66.0 ppm in a slice from ^{15}N = 115.2 ppm which displays an ~25% reduction. This suggests that it likely comes from Ile32, the succeeding residue of Pro31. However, the residual intensity of the FDR dephasing from overlapping resonances remains strong and no assignment for the Ile32 residue can be made (Fig. 4(a), right). Using the same protocol described above, the difference spectrum of Fig. 4(a, right) and Fig. 4(a, left) is shown in Fig. 4(c) (the same spectrum at a low contour level is shown in Fig. S3). A single cross-peak at 115.2 and 66.0 ppm is observed and readily assigned to Ile32.

We further tested our approach on a sample of ^{13}C, ^{15}N-labeled, Pro and Phe-unlabeled LR11 TM in *E. coli* IM vesicles (Figs. 5 and S4). A 2D REDOR-edited $^{13}C_{\alpha}$-$^{13}C'$ difference spectrum is shown in Fig. 5(a). Small amounts of ^{14}N-Phe scrambling result in slightly increased residual intensities in the spectra with dephasing on. An

Fig. 3. (a) 2D REDOR-edited $^{13}C_{\alpha}$-$^{13}C'$ correlation spectra of ^{13}C, ^{15}N-labeled, Pro-unlabeled LR11 TM in *E. coli* inner membrane vesicles acquired with REDOR dephasing off (left, blue) and on (right, red). (b) Overlays of 1D slices along the ^{13}C direct detection dimension from 2D spectra in (a), which highlight differential reductions in resonance intensity from REDOR dephasing. Peak intensities for slices from the 2D spectrum with the dephasing on (a, red) are scaled down by a factor of two relative to those from the 2D spectrum with the dephasing off (a, blue): spectrum with dephasing on was recorded with 320 scans per t_1 point, spectrum with dephasing off was recorded with 160 scans per t_1 point. (c) Left: 2D difference spectrum of two REDOR-edited $^{13}C_{\alpha}$-$^{13}C'$ correlation spectra shown in (a). The 2D spectrum with the dephasing off (a, blue) is multiplied by an empirical factor of 0.25 and then subtracted from the normalized spectrum with the dephasing on (a, red) to remove residual resonance intensities due to incomplete REDOR dephasing. Right: 1D slices along the ^{13}C direct detection dimension from the 2D difference spectrum. All spectra were recorded at a calibrated sample temperature of 305 K on a Bruker 600 MHz spectrometer. A total dephasing time of 1.33 ms was used with a MAS rate of 12 kHz. 20 rotor periods (n = 20) were used for RFDR transfer from C_{α} to C' and 16 rotor periods (Δ = 1.33 ms) were used for the Z-filter. The pulse duration for the Gaussian shape pulses was 300 μs. A recycle delay of 1.5 s was used. The 2D data were collected with 128 t_1 and 512 t_2 complex data points with spectral widths of 42.26 and 50 kHz for both F1 and F2 dimensions, respectively, and the States-TPPI was used for quadrature detection in the F1 dimension. The FIDs were apodized with a Gaussian window function with an exponential factor of −15 Hz and a Gaussian factor of 0.15 in the F1 dimension, and a Gaussian window function with an exponential factor of −20 Hz and a Gaussian factor of 0.12 in the F2 dimension, and then zero-filled into a 512 × 1024 matrix before Fourier transformation. (For interpretation of the references to colour in this figure legend, the reader is referred to the web version of this article.)

empirical factor of 0.35 (instead of 0.25 for a Pro- unlabeled sample in Fig. 3) was used to remove these residual intensities by difference spectroscopy. As expected, four $^{13}C_{\alpha}$-$^{13}C'$ cross-peaks from residues preceding unlabeled Pro and Phe are observed in the difference spectrum. Based on their characteristic $^{13}C_{\alpha}$ chemical shifts, we were able to assign specific residues. A 2D FDR-NCA difference spectrum of ^{13}C, ^{15}N-labeled, Pro and Phe-unlabeled LR11 TM in *E. coli* IM is shown in Fig. 5(b). Three of four expected ^{15}N-$^{13}C_{\alpha}$ cross-peaks (three from LR11 TM and one from the linker region of His-tag) are observed. Based on their characteristic $^{13}C_{\alpha}$ chemical shifts, we were able to obtain assignments for residues Ile32, Ala45, and Leu35 that may overlap with residue Q57 of the His-tag.

To date, we have assigned 18 of 23 LR11 TM residues using 2D ^{13}C-^{13}C correlation data and two reverse amino acid labeled samples (one with Pro/Phe unlabeled and another with Ala unlabeled). These assignments are listed in Tables 1 and S1. All assigned residues show characteristic secondary shifts of an α-helix and are in agreement with the secondary shifts of LR11 TM in DPC micelles [49]. The unassigned residues include three Leu, one Ile, and one Val. Reverse labeling of these three amino acids will introduce significant ^{14}N scrambling, but carbon is less of an issue [39,40]. Using ^{15}N-labeled Leu, Ile, or Val and the FDR-edited NCA experiment should allow us to assign three additional residues following these amino acids to achieve nearly complete backbone resonance assignments for LR11 TM.

In summary, NMR resonance assignment is a critical first step in the structural and dynamic study of membrane proteins and their complexes in biological environments. Here, we present an improved method of preparing *E. coli* IM vesicles for *in situ* ssNMR study. Our approach does not perturb the expression system and is convenient and effective. Moreover, it reduces spectral backgrounds from *E. coli* molecules and improves spectral sensitivity. Using a combination of reverse amino acid labelling, NMR spectral editing, and difference spectroscopy, we are able to surmount limitations imposed by resonance overlap and limited spectral resolution in order to successfully assign most LR11 TM residues in *E. coli*

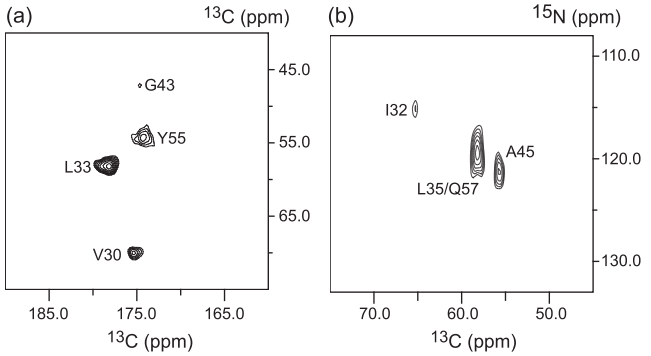

Fig. 5. (a) Difference spectra of 2D REDOR-edited $^{13}C_{\alpha}$-^{13}C (b) 2D FDR-edited ^{15}N-$^{13}C_{\alpha}$ correlation spectra of ^{13}C, ^{15}N-labeled, Pro/Phe-unlabeled LR11 TM in *E. coli* inner membrane vesicles. The spectra with dephasing off is multiplied by an empirical factor of 0.35 and then subtracted from the normalized spectra with the dephasing on to remove residual resonance intensities due to incomplete dephasing (~25%, based on Fig. 3) and small amounts of unlabeled Phe scrambling (10%). Experimental conditions for (a) and (b) were the same as described for Figs. 3 and 4, respectively.

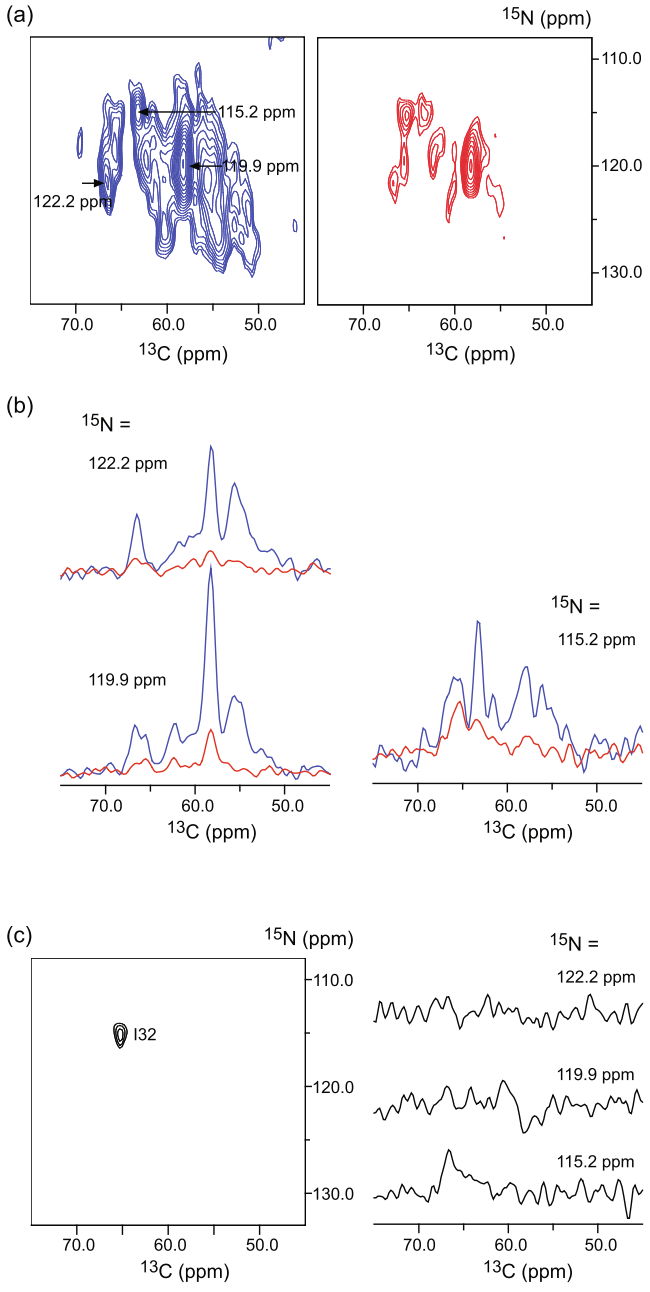

Fig. 4. (a) 2D FDR-edited ^{15}N-$^{13}C_{\alpha}$ correlation spectra of ^{13}C, ^{15}N-labelel, Pro-unlabeled LR11 TM in *E. coli* inner membrane vesicles acquired with FDR dephasing off (left, blue) and on (right, red). (b) Overlays of 1D slices along the ^{13}C dimension from 2D spectra in (a), highlighting differential reductions in resonance intensities from FDR dephasing. Peak intensities for slices from the 2D spectrum with dephasing on (a, red) are scaled down by a factor of four relative to those from the 2D spectrum with dephasing off (a, blue): spectrum with dephasing on was recorded with 1024 scans per t_1 point, spectrum with the dephasing off was recorded with 256 scans per t_1. (c) Left: 2D difference spectrum of two FDR-edited ^{15}N-$^{13}C_{\alpha}$ correlation spectra in (a). The spectrum with dephasing off (a, blue) is multiplied by an empirical factor of 0.21 and then subtracted from the normalized spectrum with the dephasing on (a, red) to remove residual resonance intensities due to incomplete FDR dephasing. Right: 1D slices along the ^{13}C dimension from the 2D difference spectrum. The spectra were recorded at a calibrated sample temperature of 305 K on a Bruker 800 MHz spectrometer. A total dephasing time of 2.57 ms was used with a MAS rate of 14 kHz. 17 rotor periods (Δ = 1.21 ms) were used for the Z-filter. A recycle delay of 1.5 s was used. The 2D data were collected with 24 t_1 and 1400 t_2 points with spectral widths of 2.919 and 100 kHz for F1 and F2 dimensions, respectively, and the TPPI method was used for quadrature detection in the F1 dimension. The FIDs were apodized with a Gaussian window function with an exponential factor of −20 Hz and a Gaussian factor of 0.12 in the F1 dimension, and a Gaussian window function with an exponential factor of −40 Hz and a Gaussian factor of 0.12 in the F2 dimension, and then zero-filled into a 256 × 1024 matrix before Fourier transformation. (For interpretation of the references to colour in this figure legend, the reader is referred to the web version of this article.)

Table 1
$^{13}C_\alpha$ chemical shifts of LR11 TM in *E. coli* inner membranes from MAS solid-state NMR.

Residue number	$^{13}C_\alpha$ (ppm)
V25	62.5
A26	55.2
A27	55.2
V28	65.6
V29	–
V30	70.0
P31	66.5
I32	66.0
L33	58.2
F34	62.8
L35	58.2
I36	–
L37	–
L38	–
S39	58.6
L40	58.3
G41	48.2
V42	66.7
G43	47.4
F44	62.5
A45	55.7
I46	65.6
L47	–

membranes. We anticipate broad applications of this approach to membrane protein-studies, especially when spectral resolution is limited.

Declaration of Competing Interest

None.

Acknowledgements

We are grateful for financial support from the National Institutes of Health NIGMS (5R01GM105963 and 1R01GM127730). This project also is funded, in part, by a grant from the Pennsylvania Department of Health Tobacco CURE Funds. The Department specifically disclaims responsibility for any analyses, interpretations, or conclusions. We thank Dr. T. A. Cross for his support and helpful discussions. Most solid-state MAS NMR measurements were performed at the National High Magnetic Field Laboratory, which is supported by the NSF Cooperative Agreement No. DMR-1644779 and the State of Florida.

Appendix A. Supplementary material

Supplementary data to this article can be found online at https://doi.org/10.1016/j.jmr.2019.106639.

References

[1] G.J. Pielak, F. Tian, Membrane proteins, magic-angle spinning, and in-cell NMR, Proc. Natl. Acad. Sci. USA 109 (2012) 4715–4716.
[2] L.S. Brown, V. Ladizhansky, Membrane proteins in their native habitat as seen by solid-state NMR spectroscopy, Prot. Sci. 24 (2015) 1333–1346.
[3] X.L. Warnet, A.A. Arnold, I. Marcotte, D.E. Warschawski, In-cell solid-state NMR: an emerging technique for the study of biological membranes, Biophys. J. 109 (2015) 2461–2466.
[4] C.G. Li, J.J. Zhao, K. Cheng, Y.W. Ge, Q. Wu, Y.S. Ye, G.H. Xu, Z.T. Zhang, W.W. Zheng, X. Zhang, X. Zhou, G. Pielak, M.L. Liu, Magnetic resonance spectroscopy as a tool for assessing macromolecular structure and function in living cells, in: R.G. Cooks, J.E. Pemberton, (Eds.), Annu. Rev. Anal. Chem., 2017, pp. 157–182.
[5] C.G. Li, M.L. Liu, Protein dynamics in living cells studied by in-cell NMR spectroscopy, FEBS Lett. 587 (2013) 1008–1011.
[6] L.A. Baker, M. Daniels, E.A.W. van der Cruijsen, G.E. Folkers, M. Baldus, Efficient cellular solid-state NMR of membrane proteins by targeted protein labeling, J. Biomol. NMR 62 (2015) 199–208.
[7] M.E. Ward, S. Wang, R. Munro, E. Ritz, I. Hung, P.L. Gor'kov, Y. Jiang, H. Liang, L. S. Brown, V. Ladizhansky, In situ structural studies of anabaena sensory rhodopsin in the E. coli membrane, Biophy. J. 108 (2015) 1683–1696.
[8] E. Barbet-Massin, A.J. Pell, J.S. Retel, L.B. Andreas, K. Jaudzems, W.T. Franks, A.J. Nieuwkoop, M. Hiller, V. Higman, P. Guerry, A. Bertarello, M.J. Knight, M. Felletti, T. Le Marchand, S. Kotelovica, I. Akopjana, K. Tars, M. Stoppini, V. Bellotti, M. Bolognesi, S. Ricagno, J.J. Chou, R.G. Griffin, H. Oschkinat, A. Lesage, L. Emsley, T. Herrmann, G. Pintacuda, Rapid proton-detected NMR assignment for proteins with fast magic angle spinning, J. Am. Chem. Soc. 136 (2014) 12489–12497.
[9] P. Fricke, V. Chevelkov, M. Zinke, K. Giller, S. Becker, A. Lange, Backbone assignment of perdeuterated proteins by solid-state NMR using proton detection and ultrafast magic-angle spinning, Nat. Protoc. 12 (2017) 764–782.
[10] Y. Ishii, J.P. Yesinowski, R. Tycko, Sensitivity enhancement in solid-state ^{13}C NMR of synthetic polymers and biopolymers by ^{1}H NMR detection with high-speed magic angle spinning, J. Am. Chem. Soc. 123 (2001) 2921–2922.
[11] Q.Z. Ni, E. Daviso, T.V. Can, E. Markhasin, S.K. Jawla, T.M. Swager, R.J. Temkin, J. Herzfeld, R.G. Griffin, High frequency dynamic nuclear polarization, Acc. Chem. Res. 46 (2013) 1933–1941.
[12] J. Medeiros-Silva, D. Mance, M. Daniels, S. Jekhmane, K. Houben, M. Baldus, M. Weingarth, ^{1}H-Detected solid-state NMR studies of water-inaccessible proteins in vitro and in situ, Angew. Chem. Int. Ed. 55 (2016) 13606–13610.
[13] M. Kaplan, S. Narasimhan, C. de Heus, D. Mance, S. van Doorn, K. Houben, D. Popov-Celeketic, R. Damman, E.A. Katrukha, P. Jain, W.J.C. Geerts, A.J.R. Heck, G.E. Folkers, L.C. Kapitein, S. Lemeer, P. Henegouwen, M. Baldus, EGFR dynamics change during activation in native membranes as revealed by NMR, Cell 167 (2017) 1241–1251.
[14] M. Kaplan, A. Cukkemane, G.C.P. van Zundert, S. Narasimhan, M. Daniels, D. Mance, G. Waksman, A. Bonvin, R. Fronzes, G.E. Folkers, M. Baldus, Probing a cell-embedded megadalton protein complex by DNP-supported solid-state NMR, Nat. Methods 12 (2015) 649–652.
[15] A.L. Paioni, M.A.M. Renault, M. Baldus, DNP and cellular solid-state NMR, Emagres 7 (2018) 51–61.
[16] T. Jacso, W.T. Franks, H. Rose, U. Fink, J. Broecher, S. Keller, H. Oschkinat, B. Reif, Characterization of membrane proteins in isolated native cellular membranes by dynamic nuclear polarization solid-state NMR spectroscopy without purification and reconstitution, Angew. Chem. Int. Ed. 51 (2012) 432–435.
[17] D.H. Zhou, A.J. Nieuwkoop, D.A. Berthold, G. Comellas, L.J. Sperling, M. Tang, G. J. Shah, E.J. Brea, L.R. Lemkau, C.M. Rienstra, Solid-state NMR analysis of membrane proteins and protein aggregates by proton detected spectroscopy, J. Biomol. NMR 54 (2007) 291–305.
[18] C. Chipot, F. Dehez, J.R. Schnell, N. Zitzmann, E. Pebay-Peyroula, L.J. Catoire, B. Miroux, E.R.S. Kunji, G. Veglia, T.A. Cross, P. Schanda, Perturbations of native membrane protein structure in alkyl phosphocholine detergents: a critical assessment of NMR and biophysical studies, Chem. Rev. 118 (2018) 3559–3607.
[19] A.A. Arnold, J.P. Bourgouin, B. Genard, D.E. Warschawski, R. Tremblay, I. Marcotte, Whole cell solid-state NMR study of Chlamydomonas reinhardtii microalgae, J. Biomol. NMR 70 (2018) 123–131.
[20] J. Medeiros-Silva, S. Jekhmane, A.L. Paioni, K. Gawarecka, M. Baldus, E. Swiezewska, E. Breukink, M. Weingarth, High-resolution NMR studies of antibiotics in cellular membranes, Nat. Commun. 9 (2018).
[21] C. Pinto, D. Mance, M. Julien, M. Daniels, M. Weingarth, M. Baldus, Studying assembly of the BAM complex in native membranes by cellular solid-state NMR spectroscopy, J. Struct. Biol. 206 (2019) 1–11.
[22] C.R. Sanders, K.F. Mittendorf, Tolerance to changes in membrane lipid composition as a selected trait of membrane proteins, Biochemistry 50 (2011) 7858–7867.
[23] X. Ding, C. Sun, H. Cui, S. Chen, Y. Gao, Y. Yang, J. Wang, X. He, D. Iuga, F. Tian, A. Watts, X. Zhao, Functional roles of tyrosine 185 during the bacteriorhodopsin photocycle as revealed by in situ spectroscopic studies, BBA Bioenerg. 2018 (1859) 1006–1014.
[24] C. Sun, X. Ding, H. Cui, Y. Yang, S. Chen, A. Watts, X. Zhao, In situ study of the function of bacterioruberin in the dual-chromophore photoreceptor archaerhodopsin-4, Angew. Chem. Int. Ed. 57 (2018) 8937–8941.
[25] Y. Miao, H. Qin, R. Fu, M. Sharma, T.V. Can, I. Hung, S. Luca, P.L. Gor'kov, W.W. Brey, T.A. Cross, M2 proton channel structural validation from full-length protein samples in synthetic bilayers and *E. coli* membranes, Angew. Chem. Int. Ed. 51 (2012) 8383–8386.
[26] P. Shi, D. Li, H.W. Chen, Y. Xiong, Y.S. Wang, C.L. Tian, *In situ* ^{19}F NMR studies of an E. coli membrane protein, Protein Sci. 21 (2012) 596–600.
[27] M. Renault, R. Tommassen-van Boxtel, M.P. Bos, J.A. Post, J. Tommassen, M. Baldus, Cellular solid-state nuclear magnetic resonance spectroscopy, Proc. Natl. Acad. Sci. USA, 109 (2012) 4863–4868.
[28] N.V. Kulminskaya, M.O. Pedersen, M. Bjerring, J. Underhaug, M. Miller, N.U. Frigaard, J.T. Nielsen, N.C. Nielsen, In situ solid-state NMR spectroscopy of protein in heterogeneous membranes: the baseplate antenna complex of chlorobaculum tepidum, Angew. Chem. Int. Ed. 51 (2012) 6891–6895.
[29] Y.X. Zhao, H.Y. Xie, L.L. Wang, Y. Shen, W. Chen, B.T. Song, Z.F. Zhang, A.M. Zheng, Q.S. Lin, R.Q. Fu, J.F. Wang, J. Yang, Gating mechanism of aquaporin Z in synthetic bilayers and native membranes revealed by solid-state NMR spectroscopy, J. Am. Chem. Soc. 140 (2018) 7885–7895.

[30] L.A. Baker, T. Sinnige, P. Schellenberger, J. de Keyzer, C.A. Siebert, A.J.M. Driessen, M. Baldus, K. Grunewald, Combined ^{1}H-detected solid-state NMR spectroscopy and electron cryotomography to study membrane proteins across resolutions in native environments, Structure 26 (2018) 161–170.
[31] R.H. Yin, J.T. Yu, L. Tan, The role of SORL1 in Alzheimer's disease, Mol. Neurobiol. 51 (2015) 909–918.
[32] T.Y. Huang, Y.J. Zhao, X.G. Li, X. Wang, I.C. Tseng, R. Thompson, S.C. Tu, T.E. Willnow, Y.W. Zhang, H.X. Xu, SNX27 and SORLA interact to reduce amyloidogenic subcellular distribution and processing of amyloid precursor protein, J. Neuronsci. 36 (2016) 7996–8011.
[33] T.E. Willnow, C.M. Petersen, A. Nykjaer, VPS10P-domain receptors - regulators of neuronal viability and function, Nat. Rev. Neurosci. 9 (2008) 899–909.
[34] T.E. Willnow, O.M. Andersen, Sorting receptor SORLA - a trafficking path to avoid Alzheimer disease, J. Cell Sci. 126 (2013) 2751–2760.
[35] R.Q. Fu, X.S. Wang, C.G. Li, A.N. Santiago-Miranda, G.J. Pielak, F. Tian, *In situ* structural characterization of a recombinant protein in native *Escherichia coli* membranes with solid-state magic-angle-spinning NMR, J. Am. Chem. Soc. 133 (2011) 12370–12373.
[36] D. Lacabanne, B.H. Meier, A. Bockmann, Selective labeling and unlabeling strategies in protein solid-state NMR spectroscopy, J. Biomol. NMR 71 (2017) 141–150.
[37] R. Verardi, N.J. Traaseth, L.R. Masterson, V.V. Vostrikov, G. Veglia, Isotope labeling for solution and solid-state NMR spectroscopy of membrane proteins, in: Isotope Labeling in Biomolecular NMR, H.S. Atreya, Editor, 2012, pp. 35–62.
[38] G.W. Vuister, S.J. Kim, C. Wu, A. Bax, 2D and 3D NMR-study of phenylalanine residues in proteins by reverse isotopic labeling, J. Am. Chem. Soc. 116 (1994) 9206–9210.
[39] C. Prasanna, A. Dubey, H.S. Atreya, Amino acid selective unlabeling in protein NMR spectroscopy, in: Z. Kelman (Ed.), Isotope Labeling of Biomolecules - Labeling Methods, 2015, pp. 167–189.
[40] P. Bellstedt, T. Seiboth, S. Hafner, H. Kutscha, R. Ramachandran, M. Gorlach, Resonance assignment for a particularly challenging protein based on systematic unlabeling of amino acids to complement incomplete NMR data sets, J. Biomol. NMR 57 (2013) 65–72.
[41] C.P. Jaroniec, B.A. Tounge, C.M. Rienstra, J. Herzfeld, R.G. Griffin, Recoupling of heteronuclear dipolar interactions with rotational-echo double-resonance at high magic-angle spinning frequencies, J. Magn. Reson. 146 (2000) 132–139.
[42] A.E. Bennett, C.M. Rienstra, P.T. Lansbury, R.G. Griffin, Frequency-selective heteronuclear dephasing by dipole couplings in spinning and static solids, J. Chem. Phys. 105 (1996) 10289–10299.
[43] T. Gullion, J. Schaefer, Rotational-echo double-resonance NMR, J. Magn. Reson. 81 (1989) 196–200.
[44] N.J. Traaseth, G. Veglia, Frequency-selective heteronuclear dephasing and selective carbonyl labeling to deconvolute crowded spectra of membrane proteins by magic angle spinning NMR, J. Magn. Reson. 211 (2011) 18–24.
[45] J.R. Banigan, A. Gayen, N.J. Traaseth, Combination of ^{15}N reverse labeling and afterglow spectroscopy for assigning membrane protein spectra by magic-angle-spinning solid-state NMR: application to the multidrug resistance protein EmrE, J. Biomol. NMR 55 (2013) 391–399.
[46] S.L. Wang, I. Matsuda, F. Long, Y. Ishii, Spectral editing at ultra-fast magic-angle-spinning in solid-state NMR: facilitating protein sequential signal assignment by HIGHLIGHT approach, J. Biomol. NMR 64 (2016) 131–141.
[47] C.P. Jaroniec, J.C. Lansing, B.A. Tounge, M. Belenky, J. Herzfeld, R.G. Griffin, Measurement of dipolar couplings in a uniformly ^{13}C,^{15}N-labeled membrane protein: Distances between the Schiff base and aspartic acids in the active site of bacteriorhodopsin, J. Am. Chem. Soc. 123 (2001) 12929–12930.
[48] J.K. Williams, K. Schmidt-Rohr, M. Hong, Aromatic spectral editing techniques for magic-angle-spinning solid-state NMR spectroscopy of uniformly ^{13}C-labeled proteins, Solid State Nucl. Magn. Reson. 72 (2015) 118–126.
[49] X. Wang, R.L. Gill, Q. Zhu, F. Tian, Bacterial expression, purification, and model membrane reconstitution of the transmembrane and cytoplasmic domains of the human APP binding protein LR11/SorLA for NMR studies, Protein Exp. Purif. 77 (2011) 224–230.
[50] A.E. Bennett, C.M. Rienstra, J.M. Griffiths, W.G. Zhen, P.T. Lansbury, R.G. Griffin, Homonuclear radio frequency-driven recoupling in rotating solids, J. Chem. Phys. 108 (1998) 9463–9479.
[51] A.E. Bennett, L.R. Becerra, R.G. Griffin, Frequency-selective heteronuclear recoupling in rotation solids, J. Chem. Phys. 100 (1994) 812–814.
[52] G. Metz, X.L. Wu, S.O. Smith, Ramped-amplitude cross-polarization in magic-angle-spinning NMR, J. Magn. Reson., Ser. A 110 (1994) 219–227.
[53] B.M. Fung, A.K. Khitrin, K. Ermolaev, An improved broadband decoupling sequence for liquid crystals and solids, J. Magn. Reson. 142 (2000) 97–101.
[54] K. Varga, L. Aslimovska, A. Watts, Advances towards resonance assignments for uniformly - ^{13}C, ^{15}N enriched bacteriorhodopsin at 18.8 T in purple membranes, J. Biomol. NMR 41 (2008) 1–4.
[55] H. Everberg, J. Clough, P. Henderson, B. Jergil, F. Tjerneld, I.B.R. Ramirez, Isolation of *Escherichia coli* inner membranes by metal affinity two-phase partitioning, J. Chromatogr. A 1118 (2006) 244–252.
[56] S. Morein, D. Henricson, L. Rilfors, Separation of inner and outer-membrane vesicles from *Escherichia coli* in self-generating Percoll gradients, Anal. Biochem. 216 (1994) 47–51.
[57] I. Yamato, Y. Anraku, K. Hirosawa, Cytoplasmic membrane vesicles of *Escherichia coli*. I. A simple method for preparing the cytoplasmic and outer membranes, J. Biochem. 77 (1975) 705–718.
[58] A. Korepanova, J.D. Moore, H.B. Nguyen, Y. Hua, T.A. Cross, F. Gao, Expression of membrane proteins from Mycobacterium tuberculosis in Escherichia coli as fusions with maltose binding protein, Prot. Exp. Purif. 53 (2007) 24–30.
[59] K. Schmidt-Rohr, K.J. Fritzsching, S.Y. Liao, M. Hong, Spectral editing of two-dimensional magic-angle-spinning solid-state NMR spectra for protein resonance assignment and structure determination, J. Bio. NMR 54 (2012) 343–353.
[60] A.E. Bennett, C.M. Rienstra, M. Auger, K.V. Lakshmi, R.G. Griffin, Heteronuclear decoupling in rotation solids, J. Chem. Phys. 103 (1995) 6951–6958.